PHYSICAL REVIEW B VOLUME 19, NUMBER 1 1 JANUARY 1979

Quantitative aspects of deuteron (spin 1) spin decoupling in solid-state NMR

D. Suwelack and M. Mehring
Institut für Physik, Universität Dortmund, 46 Dortmund, Federal Republic of Germany

A. Pines
Department of Chemistry, University of California, Berkeley, California
(Received 13 March 1978)

The dynamics of heteronuclear spin decoupling in solids is treated rigorously in the case of deuterons (^{2}D) decoupled from protons (^{1}H). Dipole-dipole interaction among each spin species is neglected. Deuteron decoupling in the presence of strong quadrupolar interaction ω_Q is governed by a double-quantum process, which is demonstrated by experiments and by double-quantum-limit calculations as compared with the rigorous treatment. Double-quantum satellites are observed in the proton NMR spectra due to coherent double-quantum motion of the deuteron spins.

I. INTRODUCTION

Heteronuclear dipolar coupling $\mathcal{H}_{IS}$ between two different spin species I and S is one of the major line-broadening mechanisms in solids. In fact, it is the main line-broadening mechanism in diluted spin systems S, where dipolar interaction among the S spins can be neglected.[1] This broadening ranges to about several kHz in solids containing abundant I spins. High-resolution S-spin magnetic resonance is therefore expected, when the I spins are decoupled by irradiation with strong rf fields at their Larmor frequency ω_{0I}.

This aspect of heteronuclear spin decoupling in solids has been of considerable interest in the past. For a review, see Ref. 2. The influence of the dipolar interaction $\mathcal{H}_{II}$ of the abudant I spins on the S-spin resonance line has been investigated more recently and interesting aspects of flip-flop spin dynamics have been demonstrated.[3] Especially the "magic angle" quenching of flip-flop terms is clearly displayed.[4] Heteronuclear spin decoupling is heavily applied in recent high-resolution NMR techniques applied to solids where high-resolution NMR spectra are obtained of either nuclei with low natural abudance [^{13}C (1.1%), ^{15}N (0.37%)] or of abundant nuclei, which are homonuclear decoupled by multiple-pulse techniques.[2,5] As an alternative technique for high-resolution NMR of protons in solids, the deuteron decoupling of highly deuterated solid samples has been proposed recently.[6] The feasibility of this approach is based on a double-quantum transition first observed by Meiboom and co-workers.[7] A review of these techniques can be found in Ref. 2. In order to achieve complete decoupling, the field strength $\omega_{1I}=\gamma_I H_1$ of the decoupling field has to be usually larger than the I-spin interactions $\|\mathcal{H}_I\|$ in the I-spin rotating frame, i.e., $\omega_{1I} \gg \|\mathcal{H}_I\|$. This condition can be achieved fairly easily if only dipolar interactions are involved. However, if $I > \frac{1}{2}$, quadrupole interactions of the I spins can be extremely large and single-quantum spin decoupling is not feasible. Even in the case of deuterons ($I=1$), the quadrupolar interaction in molecular solids is on the order of 100 kHz, which would require rf fields of more than 150 G to decouple the deuterons according to the above requirements.

Since this is technically not feasible, there seemed to be no hope for obtaining high-resolution NMR proton spectra in solids by deuteron decoupling of highly deuterated samples in the past. However, Meiboom and co-workers[7] observed that in deuterated liquid crystals a double-quantum transition allows a much more effective spin decoupling of deuterons than is expected from ordinary single-quantum transitions. These findings have been exploited recently in order to obtain high-resolution proton spectra in solids by double-quantum decoupling.[6,8] In this paper we want to derive quantitative expressions for the line shape of deuteron-decoupled spectra and we compare exact line-shape calculations with the double-quantum limit. Satellite spectra, which display the double-quantum coherence are observed for the first time and are explained quantitatively.

II. QUALITATIVE ASPECTS OF DEUTERON DECOUPLING

For the convenience of the reader, let us first repeat the simple arguments about the critical decoupling field strength ω_1^* necessary for the onset of decoupling. Suppose two different kind of spins I (with gyromagnetic ratio γ_I) and S (with gyromagnetic ratio γ_S) are coupled by dipolar interaction $\mathcal{H}_{IS}$. The secular part of the interaction Hamiltonian may then be expressed as

$$\mathcal{H}_{IS} = \sum_{i,j} B_{ij} I_{zi} S_{zj} , \tag{1}$$

with

$$B_{ij} = -2\gamma_I \gamma_S \hbar r_{ij}^{-3} P_2(\cos\vartheta_{ij}) ,$$

where r_{ij} is the distance between spins i and j and ϑ_{ij} is the angle between the vector r_{ij} and the magnetic field H_0. For simplicity we will assume just two spins, I and S, in the following, although the extension to many spins is straightforward. Later in this section when we come to the general treatment, we will relax this restriction and we will treat the many spin case rigorously. Let us discuss two different cases, namely: (i) $I=\frac{1}{2}$, $S=\frac{1}{2}$, where the resonance signal of the S spins will be observed and the I spins will be irradiated with rf fields of strength ω_1. Without irradiation of the I spins the S spin signal will have a "broadening", which is on the order of the I-S dipolar coupling, i.e.,

$$\omega_D = [\mathrm{Tr}(\mathcal{H}_{IS}^2)]^{1/2} = \tfrac{1}{2}B. \tag{2}$$

When the I spins are irradiated with an rf field ω_1 the following transition rate between $|-\frac{1}{2}\rangle$ and $|+\frac{1}{2}\rangle$ occurs:

$$W_1 = |\langle \tfrac{1}{2}|\omega_1 I_+|-\tfrac{1}{2}\rangle| = \omega_1 . \tag{3}$$

The critical field ω_1^* for the onset of decoupling is reached when

$$W_1^* = \omega_D \quad \text{or} \quad \omega_1^* = \tfrac{1}{2}B , \tag{4}$$

i.e., the strength of the rf field must be equal to the dipole-dipole interaction in order to break the coupling. (ii) $I=1$, $S=\frac{1}{2}$ where the S-spin signal will have a "broadening" ω_D according to Eq. (2) as

$$\omega_D = (\tfrac{2}{5})^{1/2} B , \tag{5}$$

with no irradiation applied to the I-spin resonance. In case the I spins have a strong quadrupole interaction, this leads to a splitting of the I-spin resonance into two lines separated by $2\omega_Q$ as shown in Fig. 1. An rf field ω_1 applied at the center frequency ω_0 cannot cause transitions from $|0\rangle$ to $|\pm 1\rangle$ unless $\omega_1 \geq \omega_Q$. Since $\nu_Q = \omega_Q/2\pi$ may reach values of 100–200 kHz for deuterons in solids, rf fields of this strength for deuterons are hardly feasible. Although the transition from $|-1\rangle$ to $|+1\rangle$ vanishes in first order, second-order perturbation theory, however, gives the expression[6-8]

$$W_2 = (2\omega_1^2/\omega_Q)|\langle 1|I_x|0\rangle\langle 0|I_x|-1\rangle| \tag{6}$$

for the transition rate from $|-1\rangle$ to $|+1\rangle$ corresponding to a double-quantum transition.

From Eq. (6), we obtain

$$W_2 = \omega_1(\omega_1/\omega_Q) \tag{7}$$

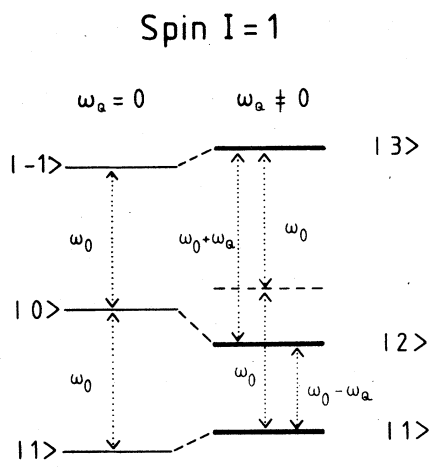

FIG. 1. Energy-level diagram of a spin 1 in a magnetic field H_0 including quadrupolar interaction ω_Q. Two satellite lines at $\omega_0 \pm \omega_Q$ are observed as a single-quantum transitions ($\Delta m = 1$). The double-quantum transition ($\Delta m = 2$) at $2\omega_0$ is indicated.

for the double-quantum transition rate, i.e., ω_1 is reduced by the factor ω_1/ω_Q in the double-quantum limit. This very important relation was already utilized in early double-quantum decoupling.[6-8] Evaluating the critical field for decoupling as in case (i) we obtain under the condition $W_2^* = \omega_D$:

$$\omega_1^*(\omega_1^*/\omega_Q) = \omega_D \quad \text{or} \quad \omega_1^* = (\omega_D\omega_Q)^{1/2} . \tag{8}$$

This equation demonstrates the efficiency of double-quantum decoupling, since only the geometric mean of ω_D and ω_Q is needed for the rf field in order to reach the critical field for decoupling.[6-8]

It will be demonstrated in the following that the double-quantum rate W_2 according to Eq. (7) imposes a coherent motion on the I spins. This motion excites "double-quantum satellites" in the S-spin spectra, as will be demonstrated in Sec. V. We shall now turn to some more general and rigorous aspects of spin decoupling with the emphasis on spin $I=1$.

III. QUANTITATIVE ASPECTS OF SPIN DECOUPLING

Let us suppose that we observe the resonance signal of dilute S spins (with $S=\frac{1}{2}$) surrounded by abundant I spins (with $I \geq \frac{1}{2}$) which will be decoupled by a strong rf irradiation ω_1, near their Larmor frequency ω_{0I}. The free-induction decay signal of the S spins after having applied a $\frac{1}{2}\pi$ pulse in the y direction of the S spin-rotating frame may be expressed as

$$G(t) = \mathrm{Tr}(e^{-it\mathcal{H}} S_x e^{it\mathcal{H}} S_x)/\mathrm{Tr}(S_x^2) \tag{9}$$

with

$$\mathcal{H} = \mathcal{H}_{1I} + \mathcal{H}_{II} + \mathcal{H}_{IS} + \mathcal{H}_{IQ} ,$$

where $\mathcal{H}$ is the total interaction Hamiltonian in the doubly rotating frame (interaction representation) and $\mathrm{Tr}\,(\,) = \mathrm{Tr}_{I,S}(\,)$ is the trace operation over I and S variables. Assuming $S = \frac{1}{2}$ and no interaction among the S spins Eq. (9) may be rewritten (after taking the trace over S)

$$G(t) = [(2I+1)^{N_I}]^{-1}\,\mathrm{Re}\,\mathrm{Tr}_I\,(e^{-i\mathcal{H}(+)t} e^{i\mathcal{H}(-)t}) , \qquad (10)$$

where N_I is the number of the I spins, Re means taking the real part of the trace, and $\mathcal{H}(\pm)$ is the interaction Hamiltonian with S_z replaced by $+\frac{1}{2}$ or $-\frac{1}{2}$, respectively. The free-induction decay $G(t)$ according to Eq. (10) cannot be calculcated rigorously if dipolar interaction among the I spins is involved. This case has been treated approximately using a memory function approach recently.[3] Here we restrict ourselves to the neglect of interactions among the I spins and of course among the S spins. In this case $[\mathcal{H}_j, \mathcal{H}_k] = 0$ for $j \neq k$ and $G(t)$ can be obtained in product form as

$$G(t) = \mathrm{Re} \prod_j (2I+1)^{-1}\,\mathrm{Tr}_I\,(e^{-i\mathcal{H}_j(+)t} e^{i\mathcal{H}_j(-)t}) . \qquad (11)$$

Let us consider some simple examples:

(i) $N_I = 1$, $I = \frac{1}{2}$; $\mathcal{H} = \omega_1 I_x + B I_z S_z$.

It follows, that

$$\mathcal{H}(\pm) = \omega_1 I_x \pm (\tfrac{1}{2}B) I_z .$$

A diagonalization of $\mathcal{H}(\pm)$ can be obtained by the transformation

$$U(\vartheta) = \exp(i\vartheta I y) ,$$

where

$$\sin\vartheta = \omega_1/\Omega; \quad \cos\vartheta = (\tfrac{1}{2}B)/\Omega$$

with the effective frequency

$$\Omega = [\omega_1^2 + (\tfrac{1}{2}B)^2]^{1/2} .$$

Insertion into Eq. (11) and evaluation of the trace leads to

$$G(t) = \sin^2\vartheta + \cos^2\vartheta \cos\Omega t . \qquad (12)$$

The limits of (no decoupling)

$$\omega_1 = 0; \quad \vartheta = 0; \quad G(t) = \cos(\tfrac{1}{2}B)t,$$

and (full decoupling)

$$\omega_1 \gg (\tfrac{1}{2}B); \quad \vartheta = \tfrac{1}{2}\pi; \quad G(t) = 1$$

are easily recovered.

In Fig. 2 we have plotted the amplitude $R = \cos^2\vartheta$ of the satellite lines at frequency Ω as a function of the decoupling field strength ω_1 in units of $\frac{1}{2}B$. Note, that a critical decoupling field ω_1^* is reached at the field strength $\frac{1}{2}B$ as obtained also from first-order perturbation theory [Eq. (4)]. R falls as ω_1^{-2} for $\omega_1 \gg \frac{1}{2}B$.

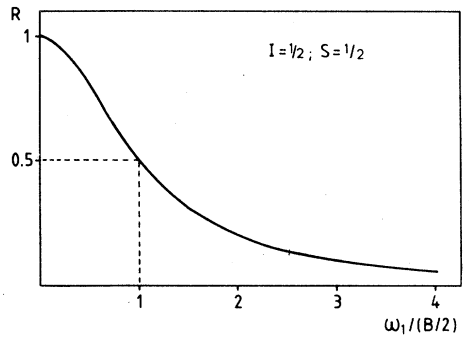

FIG. 2. Amplitude R of the satellite transition for a spin $I = \frac{1}{2}$ (single-quantum transition) [Eq. (12)] versus decoupling field strength ω_1 in units of the dipolar interaction $\frac{1}{2}B$. A "critical" field is reached at $\omega_1^* = \frac{1}{2}B$.

The extension to many I spins is straightforward and yields:

$$G(t) = \prod_j (\sin^2\vartheta_j + \cos^2\vartheta_j \cos\Omega_j t) , \qquad (13)$$

where B in the above expressions is replaced by B_j. Moreover it can be shown that $G(t)$ is independent of the phase of the rf field in the I rotating frame.

(ii) $N_I = 1$; $I = 1$; $\mathcal{H}_{QI} = 0$ (no quadrupole interaction). The same expressions for $\mathcal{H}(\pm)$ and $U(\vartheta)$ as in case (i) apply. Evaluating the trace in Eq. (11) in a similar manner as in case (i) results in

$$G(t) = \tfrac{1}{3}(1 + 6\sin^4\vartheta - 4\sin^2\vartheta + 8\sin^2\vartheta\cos^2\vartheta\cos\Omega t + 2\cos^4\vartheta\cos 2\Omega t) , \qquad (14)$$

where $\sin\vartheta$, $\cos\vartheta$, and Ω are defined as before. The following spectral lines occur:

	frequency	amplitude
central line	0	$\frac{1}{3}(1 + 6\sin^4\vartheta - 4\sin^2\vartheta)$
satellite	$\pm\Omega$	$\frac{4}{3}\sin^2\vartheta\cos^2\vartheta$
satellite	$\pm 2\Omega$	$\frac{1}{3}\cos^4\vartheta$

The limiting case $\omega_1 = 0$, $\vartheta = 0$, $G(t) = \frac{1}{3}(1 + 2\cos Bt)$ (no decoupling), and $\omega_1 \gg B$, $\vartheta \simeq \frac{1}{2}\pi$; $G(t) \simeq 1$ are easily recovered. Let us take the amplitude of the satellite at frequency 2Ω as a measure of the decoupling efficiency:

$$R = \cos^4\vartheta = 1/[1 + \omega_1^2/(\tfrac{1}{2}B)^2]^2 . \qquad (15)$$

This function is plotted versus ω_1 in Fig. 3 among other cases to be discussed later. Notice the ω_1^{-4} dependence of R for large ω_1 in contrast to the ω_1^{-2} dependence in the case of $I = \frac{1}{2}$ (Fig. 2). Again the

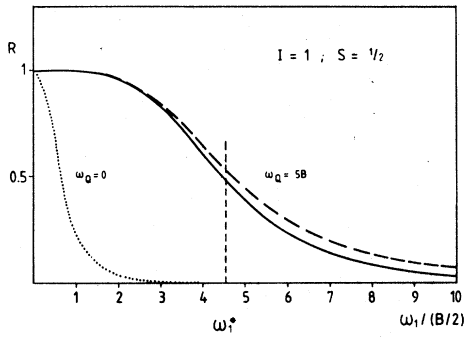

FIG. 3. Amplitude R of the strongest satellite transition for a spin $I=1$ with and without quadrupolar interaction ω_Q versus decoupling field strength ω_1. In the case $\omega_Q=0$, R is given by Eq. (15) (dotted curve), whereas for $\omega_Q\neq 0$ a rigorous [Eq. (20), (solid curve)], as well as a double-quantum limit calculation [Eq. (41), dashed curve] are compared. A critical field of $\omega_1^*\simeq 4.5(\frac{1}{2}B)$ is reached in the case $\omega_Q=5B$.

extension to many I spins is straightforward and can be written

$$G(t)=\prod_j \tfrac{1}{3}(1+6\sin^4\vartheta_j-4\sin^2\vartheta_j + 8\sin^2\vartheta_j\cos^2\vartheta_j\cos\Omega_j t + 2\cos^4\vartheta_j\cos 2\Omega_j t)\ . \tag{16}$$

(iii) $N_I=1$; $I=1$; $\mathcal{H}_Q\neq 0$.

In this case, we have

$$\mathcal{H}(\pm)=\omega_1 I_x+\tfrac{1}{3}\omega_Q[3I_z^2-I(I+1)]\pm(\tfrac{1}{2}B)I_z\ . \tag{17}$$

The diagonalization of $\mathcal{H}(\pm)$ is not as trivial as in the previous cases, although straightforward. With the transformation U_1 diagonalizing $\mathcal{H}(+)$, and U_2 diagonalizing $\mathcal{H}(-)$, the same diagonal matrix $\mathcal{H}_{\rm diag}$ results, namely,

$$U_1\mathcal{H}(+)U_1^{-1}=\mathcal{H}_{\rm diag}=U_2\mathcal{H}(-)U_2^{-1}\ , \tag{18}$$

with the eigenvalues $\lambda_1,\lambda_2,\lambda_3$. The $\mathrm{Tr}_I(\ )$ in Eq. (11) can now be expressed as

$$\mathrm{Re}\,\mathrm{Tr}_I[\exp(-it\mathcal{H}_{\rm diag})U_1U_2^{-1}\exp(it\mathcal{H}_{\rm diag})U_2U_1^{-1}] = \sum_{m,k=1,2,3} f_{mk}^2\cos(\lambda_m-\lambda_k)t\ . \tag{19}$$

This leads to the free-induction decay $G(t)$ as follows

$$G(t)=\frac{1}{3}\sum_{m,k=1,2,3} f_{mk}^2\cos(\lambda_m-\lambda_k)t\ , \tag{20}$$

where the expressions for the eigenvalues λ_j of the Hamiltonian $\mathcal{H}_{\rm diag}$ as well as the coefficients f_{mk} are given in the Appendix. The free-induction decay can thus be calculated rigorously for arbitrary values of ω_1 and ω_Q according to Eq. (20) in the limit of no dipole-dipole interaction among the deuterons and among the protons.

A typical behavior of the amplitude of the strongest satellite line with $\omega_1/(\frac{1}{2}B)$ as calculcated according to Eq. (20) is shown in Fig. 3 for $\omega_Q=5B$ (solid line). Notice that the critical field ω_1^* is reached at about 4.5 $(\frac{1}{2}B)$, which is considerably less then ω_Q.

The extension of Eq. (20) to many I spins is readily obtained as

$$G(t)=\prod_{j=1}^{NI}\left(\frac{1}{3}\sum_{m,k=1,2,3} f_{mk}^2(j)\cos(\lambda_m^{(j)}-\lambda_k^{(j)})t\right). \tag{21}$$

Summarizing, we note that the analytic expressions of the free-induction decay $G(t)$ in the cases (i)–(iii) are rigorous under the assumption of the neglect of dipolar interaction among the I spins.

In the last case (iii) the diagonalization of the interaction Hamiltonian was performed algebraically and the dynamics involved are easily lost in the procedure. We will therefore attack the problem in a different way by using fictitious spin-$\frac{1}{2}$ operators in the following.[1,9,10] In order to treat double-quantum coherence in operator form Vega and Pines[9] introduced fictitious spin-$\frac{1}{2}$ operators for the spin-1 case recently.

Instead of the Vega-Pines[9(a)] fictitious spin-$\frac{1}{2}$ operators, however, we prefer here to use the Vega[9(b)] and Wokaun-Ernst[10] operators, which refer to the basis of I_z, i.e.,

$$\begin{aligned} I_x^{r-s}&=\tfrac{1}{2}(|r\rangle\langle s|+|s\rangle\langle r|)\ ,\\ I_y^{r-s}&=-\tfrac{1}{2}i(|r\rangle\langle s|-|s\rangle\langle r|)\ ,\\ I_z^{r-s}&=\tfrac{1}{2}(|r\rangle\langle r|-|s\rangle\langle s|)\ , \end{aligned} \tag{22}$$

where $|r\rangle$ and $|s\rangle$ can take the following values

$$|1\rangle=|+1\rangle,\quad |2\rangle=|0\rangle,\quad |3\rangle=|-1\rangle\ ,$$

as shown in Fig. 1. Commutation relations and others among these operators are given in the Appendix.

The Hamiltonian $\mathcal{H}(\pm)$ in Eq. (17) may now be expressed in terms of these fictitious spin-$\frac{1}{2}$ operators as[9,10]

$$\mathcal{H}(\pm)=\pm B I_z^{1-3}+\tfrac{2}{3}\omega_Q(I_z^{1-2}-I_z^{2-3}) + \sqrt{2}\ \omega_1(I_x^{1-2}+I_x^{2-3})\ . \tag{23}$$

This Hamiltonian $\mathcal{H}(\pm)$ will now be transformed in different steps, beginning with

$$\mathcal{H}_a=\exp[(i\tfrac{1}{2}\pi)I_y^{1-3}]\mathcal{H}(\pm)\exp[(-i\tfrac{1}{2}\pi)I_y^{1-3}]\ . \tag{24}$$

After some algebraic manipulation, using the commutation relations and sum rules of the fictitious spin-$\frac{1}{2}$ operators,[9,10] $\mathcal{H}_a$ can be expressed as

$$\mathcal{H}_a = \pm BI_z^{1-3} + 2\omega_1 I_x^{1-2} + \omega_Q I_z^{1-2} + \tfrac{1}{3}\omega_Q(I_z^{2-3} - I_z^{3-1}) \ . \quad (25)$$

A diagonalization of the I^{1-2} part can now be achieved by the transformation

$$\mathcal{H}_b = \exp(i\vartheta I_y^{1-2})\mathcal{H}_a \exp(-i\vartheta I_y^{1-2}) \ , \quad (26)$$

which leads after similar algebraic manipulations as above to[10]

$$\mathcal{H}_b = \pm B(I_x^{1-3}\cos\tfrac{1}{2}\vartheta - I_x^{2-3}\sin\tfrac{1}{2}\vartheta + \tfrac{1}{2}(\omega_e - \omega_Q)I_z^{1-3} + [\tfrac{2}{3}\omega_Q + \tfrac{1}{2}(\omega_e - \omega_Q)](I_z^{1-2} - I_z^{2-3}) \ , \quad (27)$$

where

$$\sin\vartheta = 2\omega_1/\omega_e; \quad \cos\vartheta = \omega_Q/\omega_e$$

and

$$\omega_e = (4\omega_1^2 + \omega_Q^2)^{1/2} \ . \quad (28)$$

The next step in the transformation procedure is a $\frac{1}{2}\pi$ rotation of the I^{1-3} part

$$\mathcal{H}_c = \exp[(-i\tfrac{1}{2}\pi)I_y^{1-3}]\mathcal{H}_b \exp[(i\tfrac{1}{2}\pi)I_y^{1-3}] \ , \quad (29)$$

which leads to

$$\mathcal{H}_c = \pm BI_z^{1-3}\cos\tfrac{1}{2}\vartheta + \tfrac{1}{2}(\omega_e - \omega_Q)I_x^{1-3} + [\tfrac{2}{3}\omega_Q + \tfrac{1}{2}(\omega_e - \omega_Q)](I_z^{1-2} - I_z^{2-3}) \pm (2)^{-1/2}B\sin(\tfrac{1}{2}\vartheta)(I_x^{2-3} - I_x^{1-2}) \ . \quad (30)$$

If we now introduce the assumption $\omega_1 < \omega_Q$ ($\vartheta \simeq 0$) in order to neglect $\sin\frac{1}{2}\vartheta$ with respect to $\cos\frac{1}{2}\vartheta$, we reach the "double-quantum limit" and the last term in Eq. (30) can be neglected, resulting in

$$\mathcal{H}_c^* = \pm BI_z^{1-3}\cos\tfrac{1}{2}\vartheta + \tfrac{1}{2}(\omega_e - \omega_Q)I_x^{1-3} + [\tfrac{2}{3}\omega_Q + \tfrac{1}{2}(\omega_e - \omega_Q)](I_z^{1-2} - I_z^{2-3}) \ . \quad (31)$$

It is evident that $\mathcal{H}_c^*$ can immediately be diagonlized by some transformation $\exp(i\beta I_y^{1-3})$, since I_y^{1-3} commutes with $(I_z^{1-2} - I_z^{2-3})$. Before performing this step, however, we would like to discuss Eq. (31) a little further.

Note that $\mathcal{H}_c^*$ can be separated into two parts:

$$\mathcal{H}_c^* = \mathcal{H}_1^{1-3} + \mathcal{H}_2 \ , \quad (32)$$

with

$$[\mathcal{H}_1^{1-3}, \mathcal{H}_2] = 0 \ ,$$

and where the "double-quantum operator" $\mathcal{H}_1^{1-3}$ introduces transitions between levels 1 and 3.

Since $\mathcal{H}_1^{1-3}$ commutes with $\mathcal{H}_2$ we face a similar situation as in the case $\mathcal{H}_Q = 0$ [cases (i) and (ii)], but now with a double-quantum transition involved. The effective rf field strength in the double-quantum case, however, is reduced by a scaling factor ω_1/ω_Q as follows from [Eq. (31)]:

$$\tfrac{1}{2}(\omega_e - \omega_Q) \simeq \omega_1^2/\omega_Q \quad \text{when } \omega_1 \ll \omega_Q \ .$$

Note that the same result was obtained from second-order perturbation theory[6,7] [Eq. (7)], demonstrating the role of the rf field ω_1^2/ω_Q in the double-quantum frame.[9] Experimental consequences of this will be shown in Sec. V. Under the assumption $\omega_1 \ll \omega_Q$, the transformed Hamiltonian $\mathcal{H}_c^*$ in the double-quantum limit may now be rewritten

$$\mathcal{H}_c^* \simeq \pm BI_z^{1-3} + (\omega_1^2/\omega_Q)I_x^{1-3} + \tfrac{2}{3}\omega_Q(I_z^{1-2} - I_z^{2-3}) \ . \quad (33)$$

This is virtually the same Hamiltonian as $\mathcal{H}(\pm)$ in Eq. (23) where $\sqrt{2}\,\omega_1(I_x^{1-2} + I_x^{2-3})$ has been replaced by $(\omega_1^2/\omega_Q)I_x^{1-3}$ and where the $1-3$ part commutes with $(I_z^{1-2} - I_z^{2-3})$. In this limit spin dynamics introduced by the rf field is restricted to the double-quantum frame and can be treated in a simple fashion as was done in the cases (i) and (ii) ($\mathcal{H}_Q = 0$).

We now come back to the more general expression of $\mathcal{H}_c^*$ as given by Eq. (31) and perform the transformation

$$\mathcal{H}_d^* = \exp(\pm i\beta I_y^{1-3})\mathcal{H}_c^* \exp(\mp i\beta I_y^{1-3}) \ , \quad (34)$$

which leads to

$$\mathcal{H}_d^* = \pm\Omega I_z^{1-3} + [\tfrac{2}{3}\omega_Q + \tfrac{1}{2}(\omega_e - \omega_Q)](I_z^{1-2} - I_z^{2-3}) \ , \quad (35)$$

where

$$\sin\beta = [\tfrac{1}{2}(\omega_e - \omega_Q)]/\Omega^*; \quad \cos\beta = B\cos(\tfrac{1}{2}\vartheta)/\Omega^* \ , \quad (36a)$$

and

$$\Omega^* = \{(B\cos\tfrac{1}{2}\vartheta)^2 + [\tfrac{1}{2}(\omega_e - \omega_Q)]^2\}^{1/2} \ . \quad (36b)$$

In the limit $\omega_1 \ll \omega_Q$ this again reduces to

$$\sin\beta = \omega_1^2/(\omega_Q\Omega^*); \quad \cos\beta = B/\Omega^* \quad (37a)$$

with

$$\Omega^* = [B^2 + (\omega_1^2/\omega_Q)^2]^{1/2} \ . \quad (37b)$$

The Hamiltonian $\mathcal{H}_d^*$ is in diagonal form and can be readily used to calculate the trace in Eq. (11) and thus the free-induction decay. The total transformation used may be summarized as

$$U_{\text{total}} = U(\pm\beta)\,U(\vartheta) \ , \quad (38)$$

where

$$U(\vartheta) = \exp[(-i\tfrac{1}{2}\pi)I_y^{1-3}] \times \exp(i\vartheta I_y^{1-2})\exp[(i\tfrac{1}{2}\pi)I_y^{1-3}] \ , \quad (39)$$

and

$$U(\pm\beta) = \exp(\pm i\beta I_y^{1-3}) \ . \quad (40)$$

Evaluation of the trace in Eq. (11) by using the transformation U_{total} (Eq. 38) and the diagonal

Hamiltonian $\mathcal{H}_d^*$ [Eq. (35)] proceeds along the same lines as in case (ii) and results in

$$G(t) = \tfrac{1}{3}(1 + 2\sin^2\beta + 2\cos^2\beta\cos\Omega^* t)\,, \qquad (41)$$

where $\sin\beta$, $\cos\beta$, and Ω^* are given by Eq. (36) in the limit $\omega_1 < \omega_Q$ and by Eq. (37) in the limit $\omega_1 \ll \omega_Q$.

A central line with intensity $\frac{1}{3}(1+2\sin^2\beta)$ is observed together with two satellite lines at the frequency $\pm\Omega^*$ with intensity $\frac{1}{3}(\cos^2\beta)$. It is instructive to compare this double-quantum limit with the case (ii) ($\mathcal{H}_Q = 0$) and the rigorous calculation in case (iii) ($\mathcal{H}_Q \neq 0$). Especially the question arises: Is the double-quantum limit [Eq. (41)] a good enough approximation to the rigorous result [Eq. (20)] in practical cases. In Fig. 4, we have plotted spectral lines for the two different cases with the quadrupole interaction $\omega_Q = 2B$ for different parameters $\omega_1/(\frac{1}{2}B)$. Notice that only a slight difference is observed in the spectra derived from the rigorous (exact) and the double-quantum limit calculation, respectively. We have also calculated line shapes for many-spin interactions for different configurations of deuterons. In all these cases there is only a minute difference between the exact line shape according to Eq. (20) and the double-quantum limit [Eq. (41)]. Further, we would like to note that the behavior of the critical decoupling field $\omega_1^* \sim (\omega_Q\omega_D)^{1/2}$ is also displayed in Fig. 4. Similar spectra have been obtained by Emsley *et al.*[11] by means of computer diagonalization.

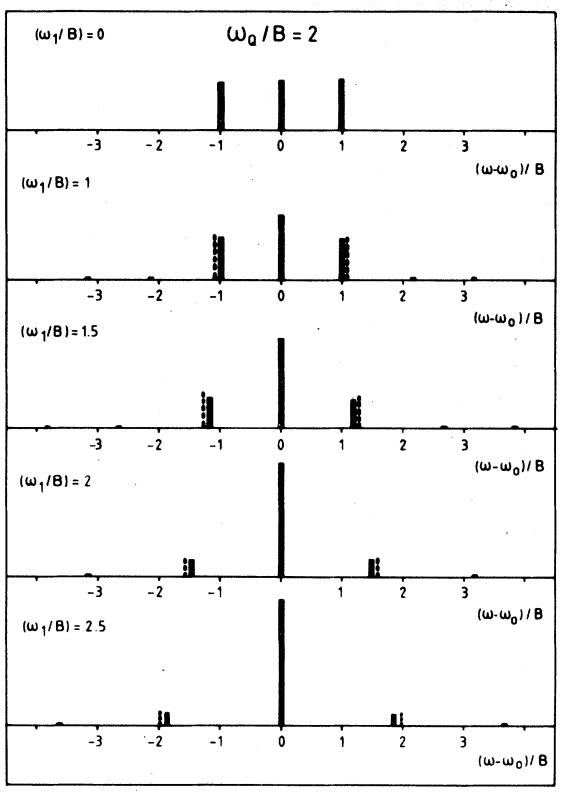

FIG. 4. Spectral lines of a spin $S = \frac{1}{2}$ coupled to a spin $I = 1$ by dipolar interaction B for different values of the decoupling field strength ω_1 applied at the Larmor frequency of the I spins. The quadrupole interaction of the I spins is fixed at $\omega_Q = 2B$. Rigorous (solid line) calculations according to Eq. (20) are compared with double-quantum limit (dashed lines) calculations according to Eq. (41). For larger ω_Q values both calculations are hardly distinguishable.

The amplitude variation of the strongest satellite lines are compared for the rigorous [Eq. (20)] and the double-quantum limit [Eq. (41)] calculations with $\omega_Q = 5B$ in Fig. 3. The overall behavior is quite similar for both calculations. Notice that the critical field $\omega_1^* \simeq 4.5\,(\frac{1}{2}B)$ is close to the value expected from second-order perturbation theory, namely [Eqs. (5) and (8)],

$$\omega_1^* = (\omega_Q\omega_D)^{1/2} = 4.04\,(\tfrac{1}{2}B)\,.$$

The deviation of the double-quantum limit calculation from the rigorous treatment decreases drastically for larger quadrupolar interaction ω_Q.

The extension to many I spins with no interaction among each other is again straightforward and is given here for completeness:

$$G(t) = \prod_j \tfrac{1}{3}\,(1 + 2\sin^2\beta_j + 2\cos^2\beta_j\cos\Omega_j^* t)\,, \qquad (42)$$

where B and ω_Q in the above expressions have to be replaced by B_j and ω_{Qj}, respectively. Free-induction decays and spectra have been calculated according to Eq. (42) and are compared with experimental data in Sec. V.

IV. EXPERIMENTAL

Experiments were performed on highly deuterated ($\geq 98\%$) hexamethylbenzene (HMB) and squaric acid (SQA) with different grades of deuteration. Single crystals were grown from aqueous solutions. The applied magnetic field was 6.3 T, which corresponds to the resonance frequency of 270 MHz for the observed proton signal and to 46.45 MHz for the decoupled deuterons.

The rf fields at both frequencies were applied to the sample in a homebuilt single coil double-resonance probehead. The 270-MHz channel was equipped with a Bruker pulse spectrometer SXP 4-100/270, whereas the decoupling channel (46.45 MHz) employed a homebuilt double resonance spectrometer. At the deuteron frequency rf fields up to 100 G could be obtained. Data

accumulation and storage was performed in a homebuilt averager and Fourier transformed by a Varian 620 L computer. All measurements were performed at room temperature.

V. RESULTS AND DISCUSSION

A representative example of the proton line shape in highly deuterated HMB is shown in Fig. 5 for a decoupling field strength of $\omega_1 = 2\pi \times 3.2$ kHz and a quadrupole interaction of $\omega_Q = 2\pi \times 8.0$ kHz. HMB has the interesting property, that all deuterons in the unit cell are magnetically equivalent due to rapid molecular reorientation, i.e., only a single value of the quadrupole interaction ω_Q is observed, depending on the angle β of the molecular sixfold axis with respect to the magnetic field as

$$\omega_Q = \tfrac{1}{2}(3\cos^2\beta - 1)\,\omega_{Q0}, \tag{43}$$

where $\omega_{Q0} = 2\pi \times 16.2$ kHz in HMB.

The theoretical line shape was calculated using the given molecular and crystal structure together with the measured value for the quadrupole interaction ω_Q. No detectable difference between the exact [Eq. (21)] and the double-quantum limit [Eq. (42)] calculation was observed.

In Fig. 5 we compare the calculated and the experimental line shape and find a fairly good agreement. Note the satellite peaks in Fig. 5, which are due to the coherent spin motion caused

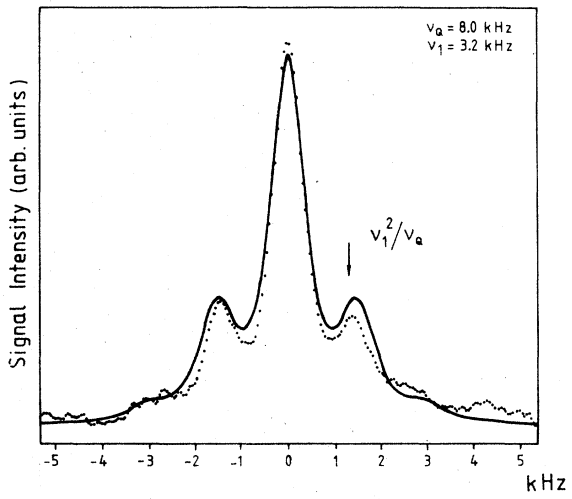

FIG. 5. Proton-resonance spectra (dotted curve) at 270 MHz of highly deuterated (≥ 98%) hexamethylbenzene (HMB) for $\nu_Q = 8.0$ kHz and $\nu_1 = 3.2$ kHz. The theoretical line shape (solid curve) was calculated according to Eq. (21) (rigorous) as well as Eq. (42) (double-quantum limit) by using the molecular and crystal structural data together with the values for ω_Q and ω_1 as given above. Notice the "double-quantum satellites" at about ν_1^2/ν_Q.

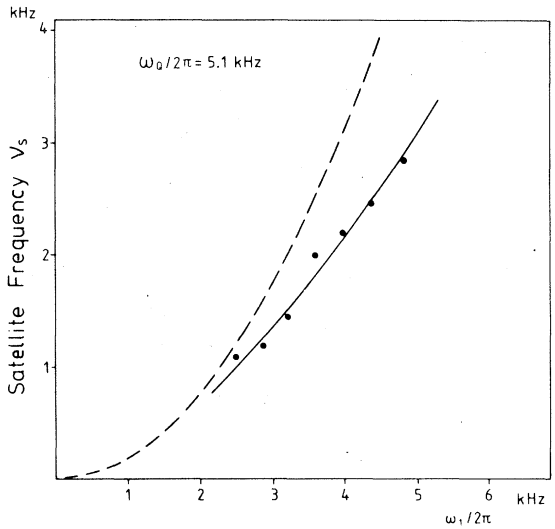

FIG. 6. Double-quantum satellite frequency ν_s as obtained from spectra like Fig. 5 versus decoupling field ω_1. The theoretical curve (solid line) derives from line-shape calculations like in Fig. 5, whereas the dashed line represents the simple relation $\nu_s = \nu_1^2/\nu_Q$.

by the double-quantum transition with a rate of about ω_1^2/ω_Q. The satellite frequency ν_s as obtained from similar spectra for different values of ω_1 is plotted versus ω_1 in Fig. 6. The theoretical curve (solid line) in Fig. 6 derives from calculated line shapes as shown in Fig. 5. The agreement with the experimental data is quite pleasing. Also the rough estimate of the satellite frequency ν_s by ω_1^2/ω_Q (dashed line) shows the correct trend.

In order to investigate the decoupling efficiency we have measured the linewidth of the proton resonance line in HMB for different decoupling fields ω_1. Typical results for two different ω_Q values are plotted in Fig. 7, together with the theoretically determined normalized linewidth δ_n. The calculations were done rigorously [Eq. (21)] as well as in the double-quantum limit [Eq. (42)] with no noticeable difference in Fig. 7. Note also the rapid decrease of the linewidth once the critical field ω_1^* is reached. This behavior was also demonstrated in the coherent average approach as used previously.[6] From the simple formula [Eq. (8)], the critical field should be proportional to $(\omega_Q\omega_D)^{1/2}$. We have therefore plotted ω_1^* versus $(\omega_Q\omega_D)^{1/2}$ in Fig. 8. Different values of ω_Q and ω_D were obtained by different orientations of the HMB crystal in the magnetic field. The critical field ω_1^* was obtained from plots like Fig. 7. The calculated curve (solid line) follows from rigorous as well as double-quantum limit calculations and represents the data quite accurately. The simple expression $\omega_1^* = (\omega_Q\omega_D)^{1/2}$ (dashed line) obtained from second-order perturbation theory

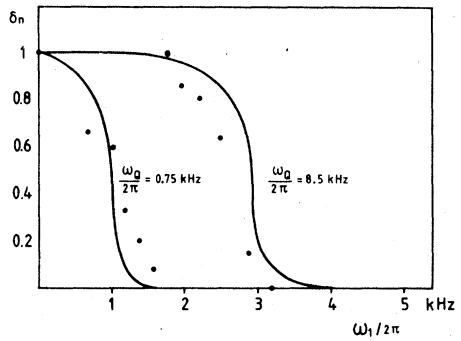

FIG. 7. Normalized linewidth δ_n of proton spectra in deuterated HMB versus decoupling field ω_1 for different values of the quadrupole interaction ω_Q of the deuterons. The theoretical curves (solid lines) are obtained by taking the linewidth of spectra, which were calculated rigorously [Eq. (21)] as well as in the double-quantum limit [Eq. (42)], with both calculations leading to indistinguishable results on the scale of the drawing.

does show the general trend, but deviates from the experimental data appreciably.

Finally, we want to demonstrate again that this technique might be useful for obtaining high-resolution proton NMR spectra in solids, by showing the deuteron decoupled proton spectrum in highly deuterated squaric acid ($C_4O_4D_2$), where the proton chemical shift tensor has been determined previously[12] (see Fig. 9). The residual proton linewidth was investigated for different grades of dilution in this compound. An account of this will be reported later.

VI. CONCLUSION

Proton line broadening of diluted protons immersed in a deuterated matrix can be calculated quantitatively for arbitrary strength of the decoupling field ω_1. The spin dynamical process involved is a double-quantum transition, which makes the decoupling very efficient. Line-shape calculations show that only minute differences occur for rigorous and double-quantum limit calculations. Coherent spin motion due to the double-quantum transitions is observed as "double-quantum satellites" in the proton spectra. All these phenomena can be accounted for quantitatively.

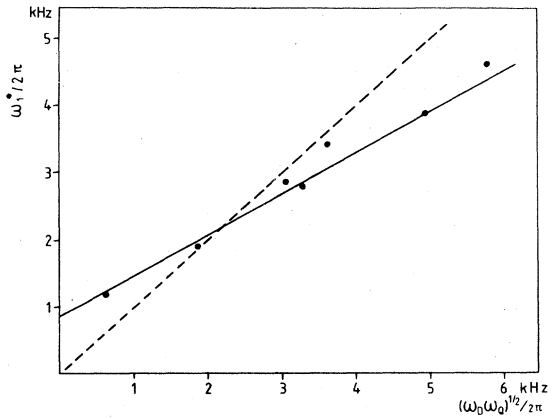

FIG. 8. Critical decoupling field ω_1^* ($\delta_n = \frac{1}{2}$) as obtained from data like those presented in Fig. 7 versus $(\omega_Q\omega_D)^{1/2}$. The theoretical line (solid line) derives from critical fields ω_1^* at $\delta_n = \frac{1}{2}$ as obtained from similar theoretical curves as in Fig. 7.

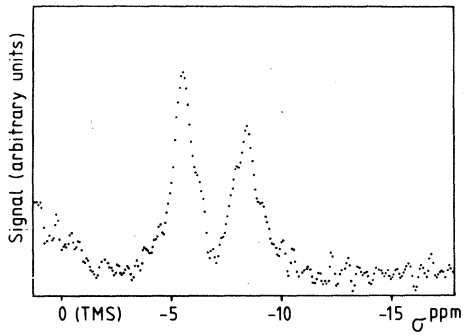

FIG. 9. High-resolution proton spectra at 270 MHz in highly deuterated (99%) squaric acid by deuteron decoupling. Shift values σ are given with respect to TMS.

ACKNOWLEDGMENTS

The single crystal of HMB was kindly grown by H. Zimmermann. Intensive discussions with Dr. S. Vega on double-quantum decoupling is gratefully acknowledged. We would also like to thank J.D. Becker for his help in taking the experimental data. The Deutsche Forschungsgemeinschaft has given considerable financial support.

APPENDIX

A. Diagonalization of $\mathcal{H}(\pm)$

We have

$$\mathcal{H}(\pm) = \omega_1 I_x + \tfrac{1}{3}\omega_Q [3I_z^2 - I(I+1)] \pm (\tfrac{1}{2}/B) I_z . \quad \text{(A1)}$$

Diagonalization of $\mathcal{H}(\pm)$ is achieved by the transformation

$$U_1 \mathcal{H}(+)\, U_1^{-1} = \mathcal{H}_{\text{diag}} = U_2 \mathcal{H}(-)\, U_2^{-1} , \quad \text{(A2)}$$

where

$$U_1 = \begin{pmatrix} r_{11} & r_{12} & r_{13} \\ r_{21} & r_{22} & r_{23} \\ r_{31} & r_{32} & r_{33} \end{pmatrix} ;$$

$$U_2 = \begin{pmatrix} -r_{13} & -r_{12} & -r_{11} \\ r_{23} & r_{22} & r_{21} \\ r_{33} & r_{32} & r_{31} \end{pmatrix} , \quad \text{(A3)}$$

with

$$r_{il} = r'^2_{ik} \Big/ \Big(\sum_{k=1}^{3} r'^2_{ik} \Big)^{1/2}, \quad i,l = 1,2,3, \tag{A4}$$

and

$$\begin{aligned}
r'_{11} &= \lambda_2 \lambda_3 - (\lambda_2 + \lambda_3) Q_- + Q_-^2 + \tfrac{1}{2}\omega_1^2, \\
r'_{12} &= -\omega_1(\lambda_2 + \lambda_3 + Q_+)/\sqrt{2}, \\
r'_{13} &= \tfrac{1}{2}\omega_1^2, \\
r'_{21} &= -\omega_1(\lambda_1 + \lambda_3 + Q_+)/\sqrt{2}, \\
r'_{22} &= \lambda_1 \lambda_3 + \tfrac{2}{3}\omega_Q(\lambda_1 + \lambda_3) + \omega_1^2 + \tfrac{4}{9}\omega_Q^2, \\
r'_{23} &= -\omega_1(\lambda_1 + \lambda_3 + Q_-)/\sqrt{2}, \\
r'_{31} &= \tfrac{1}{2}\omega_1^2, \\
r'_{32} &= -\omega_1(\lambda_1 + \lambda_2 + Q_-)/\sqrt{2}, \\
r'_{33} &= \lambda_1 \lambda_2 - (\lambda_1 + \lambda_2) Q_+ + Q_+^2 + \tfrac{1}{2}\omega_1^2/2,
\end{aligned} \tag{A5}$$

with

$$Q_\pm = \tfrac{1}{3}\omega_Q \pm \tfrac{1}{2} B .$$

The eigenvalues λ_1, λ_2, λ_3 of $\mathcal{H}_{\text{diag}}$ are then given by

$$\begin{aligned}
\lambda_1 &= -2p\cos(\tfrac{1}{3}\varphi + 60^\circ), \\
\lambda_2 &= -2p\cos(\tfrac{1}{3}\varphi - 60^\circ), \\
\lambda_3 &= 2p\cos(\tfrac{1}{3}\varphi),
\end{aligned} \tag{A6}$$

with

$$\cos\varphi = -q/p^3, \tag{A7}$$

$$p = [(\tfrac{1}{3}\omega_Q)^2 + \tfrac{1}{3}(\tfrac{1}{2}B)^2 + \tfrac{1}{3}\omega_1^2]^{1/2}, \tag{A8}$$

$$q = (\tfrac{1}{3}\omega_Q)\,[(\tfrac{1}{3}\omega_Q)^2 - (\tfrac{1}{2}B)^2 + \tfrac{1}{2}\omega_1^2]. \tag{A9}$$

From Eq. (19), $G(t)$ follows readily:

$$G(t) = \frac{1}{3} \sum_{m,k=1,2,3} f_{mk}^2 \cos(\lambda_m - \lambda_k) t, \tag{A10}$$

where λ_1, λ_2, and λ_3 are given by Eqs. (A6)–(A9) and where

$$F = \{f_{mk}\} = U_2 U_1^{-1}. \tag{A11}$$

F. Fictitious spin-½ operators for $I = 1$ in the Vega-Wokaun-Ernst notation (Refs. 9 and 10)

$$\begin{aligned}
I_x^{r-s} &= \tfrac{1}{2}(|r\rangle\langle s| + |s\rangle\langle r|), \\
I_y^{r-s} &= -\tfrac{1}{2} i(|r\rangle\langle s| - |s\rangle\langle r|), \\
I_z^{r-s} &= \tfrac{1}{2}(|r\rangle\langle r| - |s\rangle\langle s|),
\end{aligned} \tag{A12}$$

with

$$I_x^{s-r} = I_x^{r-s}; \quad I_y^{s-r} = -I_y^{r-s}; \quad I_z^{s-r} = -I_z^{r-s}. \tag{A13}$$

For the convenience of the reader, we summarize some of the relations of the operators I_α^{r-s}, $\alpha = x,y,z$ following Wokaun-Ernst[10] (for $I = 1$):

$$I_{x,y} = \sqrt{2}\,(I_{x,y}^{1-2} + I_{x,y}^{2-3}), \tag{A14}$$

$$I_z = 2(I_z^{1-2} + I_z^{2-3}), \tag{A15}$$

and with

$$I_z^{1-2} + I_z^{2-3} + I_z^{3-1} = 0, \tag{A16}$$

follows

$$I_z = I_z^{1-2} + I_z^{2-3} + I_z^{1-3} = 2 I_z^{1-3}. \tag{A17}$$

The following commutation rules apply:

$$(I_\alpha^{r-s}, I_\beta^{r-s}) = i I_\gamma^{r-s}, \quad \alpha,\beta,\gamma = x,y,z \text{(cyclic)} \tag{A18}$$

and

$$\begin{aligned}
&[I_x^{r-t}, I_x^{s-t}] = [I_y^{r-t}, I_y^{s-t}] = (\tfrac{1}{2}i) I_y^{r-s}, \\
&[I_x^{r-t}, I_y^{s-t}] = (\tfrac{1}{2}i) I_x^{r-s}, \\
&[I_x^{r-t}, I_z^{st}] = (-\tfrac{1}{2}i) I_y^{r-t}, \\
&[I_y^{r-t}, I_z^{s-t}] = (\tfrac{1}{2}i) I_x^{r-t}, \\
&[I_z^{r-t}, I_z^{s-t}] = 0,
\end{aligned} \tag{A19}$$

where r,s,t are all unequal.

[1] A. Abragam, *Principles of Nuclear Magnetism* (Oxford U.P., London, 1961).
[2] M. Mehring, in *NMR: Basic Principles and Progress* (Springer, Berlin, 1976), Vol. 11.
[3] M. Mehring and G. Sinning, Phys. Rev. B 15, 2519 (1977).
[4] M. Mehring, G. Sinning, and A. Pines, Z. Phys. B 24, 73 (1976).
[5] U. Haeberlen, Adv. Magn. Reson. Supp. (Academic, New York, 1976).
[6] A. Pines, D. J. Ruben, S. Vega, and M. Mehring, Phys. Rev. Lett. 36, 110 (1976).
[7] R. C. Hewitt, S. Meiboom, and L. C. Snyder, J. Chem. Phys. 58, 5089 (1973); L. C. Snyder and S. Meiboom, *ibid.* 58, 5096 (1973).
[8] A. Pines, S. Vega, and M. Mehring, Phys. Rev. (to be published).
[9] (a) S. Vega and A. Pines, J. Chem. Phys. 66, 5624 (1977); (b) S. Vega (to be published).
[10] A. Wokaun and R. R. Ernst, J. Chem. Phys. 67, 1752 (1977).
[11] J. W. Emsley, J. C. Lindon, and J. M. Tabong, J. Chem. Soc. Faraday Trans. 2 69, 10 (1973).
[12] D. Suwelack, J. D. Becker, and M. Mehring, Solid State Commun. 22, 597 (1977).